Geophysical Research Letters

Supporting Information for

Snow Crash: Compaction craters on (486958) Arrokoth and other small KBOs

William B. McKinnon[1], Xiaochen Mao[1], P. M. Schenk[2], K. N. Singer[3], S. J. Robbins[3], O. L. White[4,5], R. A. Beyer[4,5], S. B. Porter[3], J. T. Keane[6], D. T. Britt[7], J. R. Spencer[3], W. M. Grundy[8,9], J. M. Moore[6], S. A. Stern[3], H. A. Weaver[10], C. B. Olkin[3], and the New Horizons Science Team

[1]Department of Earth and Planetary Sciences and McDonnell Center for the Space Sciences, Washington University in St. Louis, St. Louis, MO, USA, [2]Lunar and Planetary Institute, Houston, TX, USA, [3]Southwest Research Institute, Boulder, CO, USA, [4]SETI Institute, Mountain View, CA, USA, [5]Space Science Division, NASA Ames Research Center, Moffett Field, CA, USA, [6]Jet Propulsion Laboratory, California Institute of Technology, Pasadena, CA, USA, [7]Department of Physics, University of Central Florida, Orlando, FL, USA, [8]Lowell Observatory, Flagstaff, AZ, USA, [9]Department of Astronomy and Planetary Science, Northern Arizona University, Flagstaff, AZ 86011, USA, [10]Space Department, Johns Hopkins University Applied Physics Laboratory, Laurel, MD, USA

Contents of this file

Introduction

Text S1 and Figure S1 provide supporting details on the likely compressive strength of Arrokoth and other small, more-or-less pristine KBOs (highly collisionally evolved KBOs being different). Text S2 quantifies the potential implications of using the minimum published comet/KBO crush strength. Text S3 provides additional explanation of published crater size-frequency analyses discussed in Section 5.2 of the main text. Text S4 provides supporting details for the temperature estimates in Section 5.3 of the main text. Figures S2, S3, and S5 provide further background on the compaction crater concept and its scaling. Figure S4 illustrates the potential effect of compaction cratering on Arrokoth's spin evolution, whereas Figures S6 and S7 further illustrate the implications of compaction cratering during the formation of Sky crater on Arrokoth.

Text S1. On the minimum bulk compressive strength of comet 67P/Churyumov-Gerasimenko.

O'Rourke et al. (2020) recently determined the compressive strength of a boulder on comet 67P to be ≲12 Pa, which is extraordinarily low, weaker than freshly fallen snow (e.g., Wang et al., 2021). The applicability of this value to 67P as a whole or to small KBOs generally is, however, problematic. This strength measure was determined by estimating the thermodynamic *P*d*V* work done by the impact and rebound of the Philae lander. The minimum volume of the "skull face" indent on the 67P boulder caused by the Philae bounce was estimated as 0.054 ± 0.011 m^3 and the decrease in the lander's kinetic energy as 0.67 ± 0.30 J, their ratio yielding 12 ± 6 Pa (O'Rourke et al., 2020).

In contrast, the shear face of the Hathor cliff on the side of the head of comet 67P, facing the main body of the comet, is 900 m tall, and implies a minimum compressive strength of 50 Pa (Figure S1). Groussin et al. (2015) and Basilevsky et al. (2016) find the cliff slope in Figure S1 to be ~75°, so vertical compressive stresses σ at the base of the cliff reach values of $\int_0^h \rho g(z)\sin(75°)\mathrm{d}z$, which for ρ = 500 kg m^{-3}, mean effective gravity $g \sim 1.2 \times 10^{-3}$ m s^{-2} (see Figure 13 in Pajola et al., 2015), and h = 900 m gives $\sigma \sim$ 50 Pa. From the structural stability at the base of the Hathor cliff, the unconfined compressive strength (σ_c) of comet 67P *in bulk* must be at least this much.

Text S2. Compaction cratering at the extreme low crush-strength limit

If we were to adopt the very low 12 Pa strength limit of O'Rourke et al. (2020) for comet 67P as Y_c, then all craters observed on Arrokoth would have formed as essentially ejecta-less compaction craters. But as discussed above, this strength is unlikely to apply to 67P in bulk (it's too low). Moreover, 12 Pa of overburden is reached on Arrokoth at modest depths of 24 m × (500 kg m^{-3}/ρ)^2, for a uniform density Arrokoth. In other words, 12 Pa is not a possible crush strength for the bulk of Arrokoth; the body's internal porosity would already have been crushed out by at least 50%. But this does bring up the interesting possibility that there may be porosity and thus density gradients within the two lobes of Arrokoth, if Y_c is low enough.

Text S3. Small crater size-frequency distributions on Pluto and Charon

Robbins & Singer (2021) performed an in-depth analysis of Pluto and Charon crater data, including a completely new crater mapping exercise and a detailed discussion of fitting methods for SFD slopes. Table 1 of their work summarizes the results, where different terrains' craters on both Pluto and Charon are fit with multiple diameter ranges. To represent small craters (of interest here), two different maximum values were used (10 km and 12 km), while the minimum diameter was variable based on estimated completeness of the counts. From that Table, one general trend is that Robbins' craters tend to yield slightly steeper slopes than Singer's, but the values for every terrain are within each others' uncertainty.

Their paper dicussed what terrain was most likely to yield the most reliable SFD power-law slope, rejecting Pluto due to extensive terrain modification, and focusing in particular on the high-resolution LORRI data across Charon's Vulcan Planitia. Finding no clear evidence that the crater SFD transition was as small as 10 km in that area, they preferred slopes using the maximum diameter of 12 km, which Singer's craters yielded a slope of –1.6±0.2 and Robbins' –1.8±0.2. A weighted mean when carrying out the calculation to more decimal points yielded a

slope of –1.7±0.2, which is what they prefer as the most likely representation of the small crater SFD in the Pluto system and which agrees with earlier work by Singer et al. (2019).

While there is a non-trivial range of other slopes in their Table 1, there is also an extensive discussion in their paper about what is believable and what are reasonable uncertainties: They pointed out that when dealing with these relatively few craters (~tens), inclusion or omission of even a single crater could change the slope by ±0.1. So, while one could pick a preferred value from that Table, one must take the work in context and appreciate the uncertainties, balanced against what is most likely given what we know about geologic context and the images upon which the counts are based.

Text S4. Thermal effects of compaction crater formation.

The so-called "waste heat" due to impact-driven compaction is well approximated by $\frac{1}{2}P_s(V_o - V_s)$, where P_s is the shock pressure and V_o and V_s are original (uncompressed) and shocked specific volume (1/density) (e.g., Kieffer & Simonds, 1980). The shock pressure is given by the Rankine-Hugoniot relation $P_s = \rho_o u_p U_s$, where ρ_o is the unshocked density, and u_p and U_s are the post-shock particle and shock speeds, respectively.

For like-on-like impacts in the Kuiper belt, the material particle speed in the target is exactly ½ the impact velocity. For cold classical KBOs the characteristic impact velocity (U) is ~300 m s^{-1} (Greenstreet et al., 2019), which for an average impact angle of 45° translates into a vertical or normal impact velocity of ~200 m s^{-1} and u_p ~100 m s^{-1}. For dynamically hot classicals, which impact at ~1400 m s^{-1}, the implied normal particle speed is ~500 m/s. Scattered disk objects, which nominally are unimportant for cratering Arrokoth today, could have been dominant in the immediate aftermath of the planetary dynamical instability that created (populated) the Kuiper belt (Morbidelli et al., 2021); scattered disk objects today have a characteristic U at Arrokoth of ~2700 m s^{-1} (Greenstreet et al., 2019), implying a vertical u_p of ~950 m s^{-1}. With these estimates and a plausible density range for Arrokoth (250 to 500 kg m^{-3}), the remaining major unknown is the shock speed U_s.

We can, however, quickly estimate the scale of the heating through dimensional analysis, substituting the vertical impact speed for both u_p and U_s in the Rankine-Hugoniot relation:

$$P_s = \frac{1}{2}\rho_o U^2 \quad . \qquad \text{(S1)}$$

For U = 300 (1400) m s^{-1}, P_s = 22 (490) MPa, which for an initial density ρ_o = 500 kg m^{-3} gives an increase in specific energy ΔE of 16 (350) kJ kg^{-1}, assuming complete crush-up (no residual porosity) upon unloading (density = 1800 kg m^{-3}, based on that of the Pluto system). ΔE values assuming ρ_o = 250 kg m^{-3} are similar. McKinnon et al. (2021) derived a formula for the temperature-dependent heat capacity of KBO solids, referenced to 40 K, 1150 × (T/250 K) J kg^{-1} K^{-1}. For this heat capacity, ΔE = 16 kJ kg^{-1} implies a temperature increase from 40 to ~90 K, whereas 350 kJ kg^{-1} implies heating to 273 K with enough left over to melt all the water ice in the KBO dust+ice mix.

Better estimates require more detailed knowledge of the Hugoniot for highly porous granular solids, which is generally lacking in the velocity range of interest here. For example, Bakanova et al. (1976) measured shock speeds in highly porous granular ice (ρ_o = 350 kg m^{-3}) and determined $u_p = 1.425U_s$, but as their lowest measured particle speed was 2.76 km s^{-1}, considerable extrapolation is required for much lower u_p. More realistically, at low shock compressions (a few MPa), the highly porous framework of a KBO surface should collapse to

something more resembling (structurally) a dense sand (in vacuo) or deep lunar regolith. From Apollo seismic studies (Cooper et al., 1974) and laboratory experiments (Stesky, 1978), we expect P-wave and hence shock speeds of order 1 km s^{-1}. For U_s = 1 km s^{-1}, ρ_o = 500 kg m^{-3}, and the characteristic cold and hot classical KBO impact speeds above, estimated shock pressures are 50 (250) MPa, and specific ΔE gains are 35 (180) kJ kg^{-1}. Compared with the simpler estimate above, the ΔT for impacting cold classical bodies may be somewhat greater (reaching ~130 K), whereas hot classical impacts result in ΔT that ~just reach 273 K.

The above estimates illustrate the range of uncertainty in temperature increases due to impact conditions in the cold classical Kuiper belt (CCKB). But it seems reasonable to conclude that collisions of CCKBOs with bodies like Arrokoth will result in modest temperature increases, despite the well-known efficiency of waste heat generation during shock compression of porous solids. Free supervolatile ices such as CH_4, CO, and N_2 will be mobilized, but clathrates and amorphous water ice (which may contain occluded volatiles) should remain stable due to the limited time the shocked lens of impactor and target (Figure S2) remains warm due to diffusive heat loss to surrounding, much colder material. Higher impact speeds may reach or exceed the water-ice melting threshold, but any water produced will rapidly refreeze. In both cases, the shock crushed lens should be somewhat sintered if not cemented.

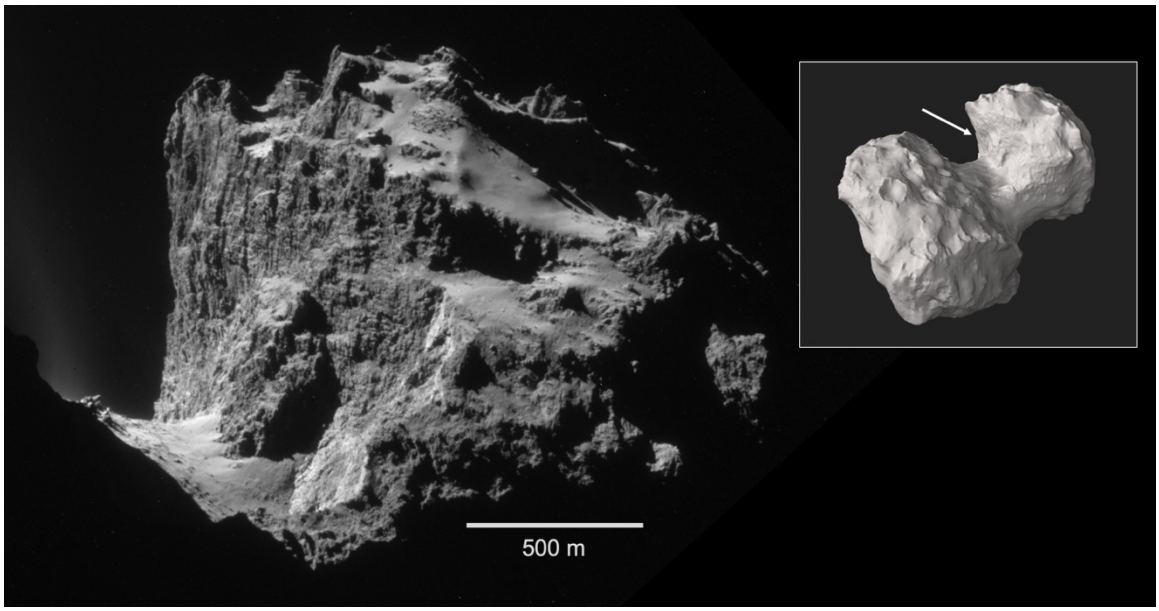

Figure S1. Hathor cliff on comet 67P/Churyumov-Gerasimenko (see inset NavCam shape model for location). Portion of *Rosetta* NavCam image 20141106T202256; shape model from http://open.esa.int/rosetta-3d-model.

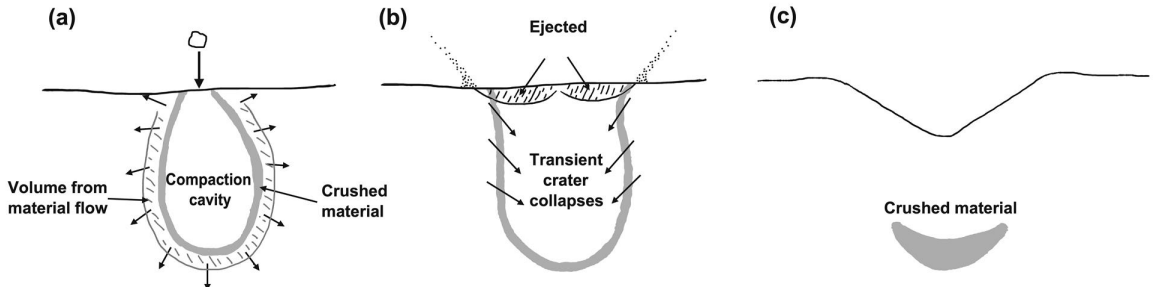

Figure S2. Schematic illustration of crater formation in highly porous materials. From Housen et al. (2018), reproduced with kind permission. Note that the deep ovoid-shaped cavity illustrated is influenced by the experiments described in Housen et al. (2018), which generally have very high impactor/target density ratios δ/ρ. For primordial KBO impacts, δ/ρ is likely much closer to 1, and the depth of penetration by the impactor could be markedly less. For cold classical impactors at ~300 m s^{-1}, the depth of penetration should be about 2.5 impactor diameters; for scattered disk impactors at ~1400 m s^{-1} the penetration depth increases to ~5 impactor diameters (see Fig. 10 in Housen et al. 2018).

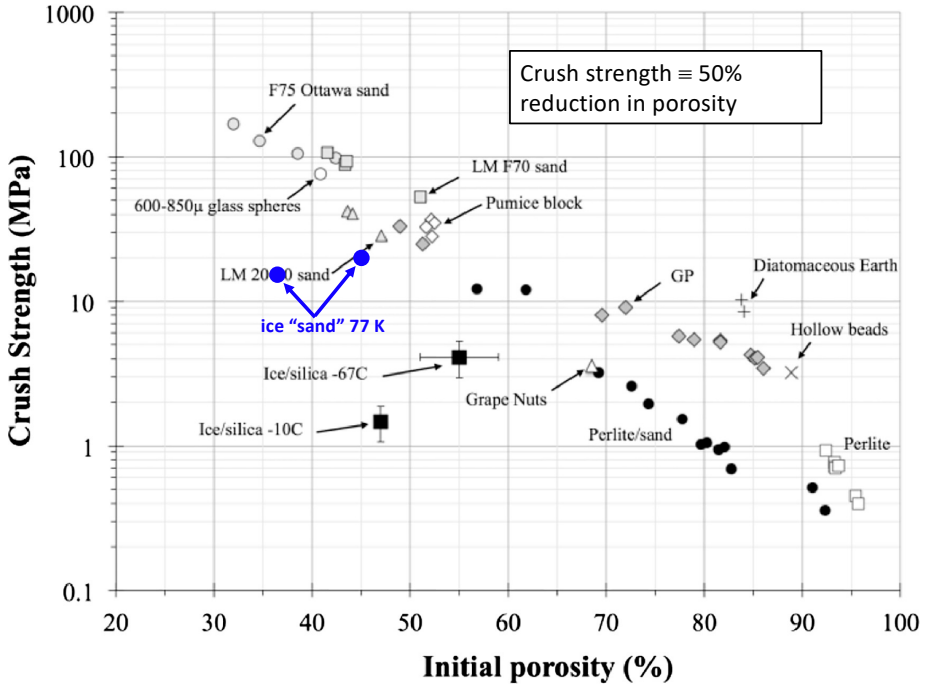

Figure S3. Crush strength of various granular aggregates as a function of porosity. The crush strength for highly porous, icy KBOs such as Arrokoth (>70% porosity) is plausibly well under 1 MPa. From Housen et al. (2018) with granular water ice (ice "sand") points from Durham et al. (2005).

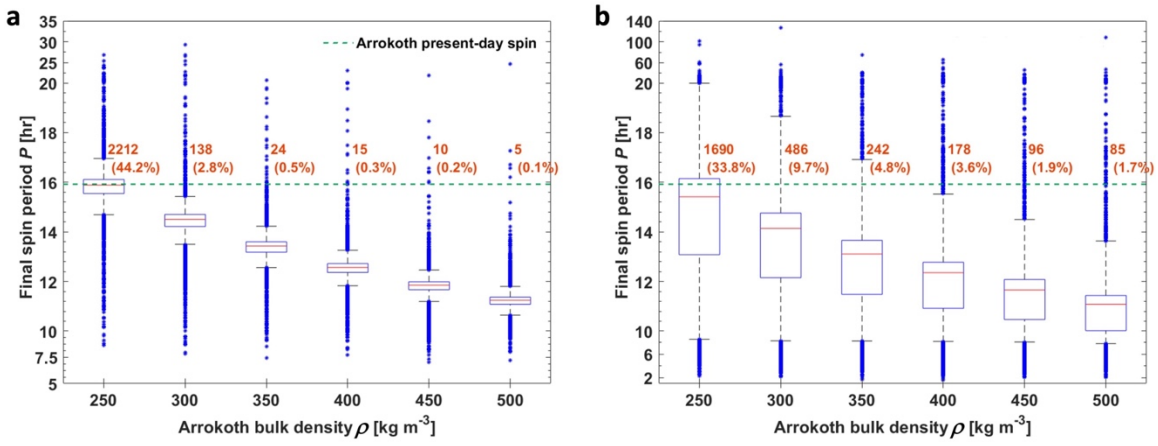

Figure S4. (a) Boxplots of Arrokoth's spin distributions as a function of initial density and spin period chosen to minimize neck stress. Red lines are the median values in each suite of Monte Carlo simulations, the box height equals the interquartile range (IQR), and the whisker length is 1.5×IQR. Green dashed line indicates Arrokoth's observed spin (15.92 hr). These simulations assume 100% ejecta retention and can be compared with results in Mao et al. (2021). Blue points are outliers of the Lorentzian

distributions of final spins, and red values are the number (percentage) of simulations (out of 5000 in each case) whose final spin period matched or exceeded that of Arrokoth today. As discussed in Mao et al. (2021), modeled Kuiper belt impactor size-frequency and velocity distributions follow Singer et al. (2019) and Greenstreet et al. (2019), respectively, with an upper limit impactor diameter d_{max} = 1 km. (b) Similar to panel a but with d_{max} = 2 km. In those few cases where catastrophic disruption is triggered, the prior spin is the final spin.

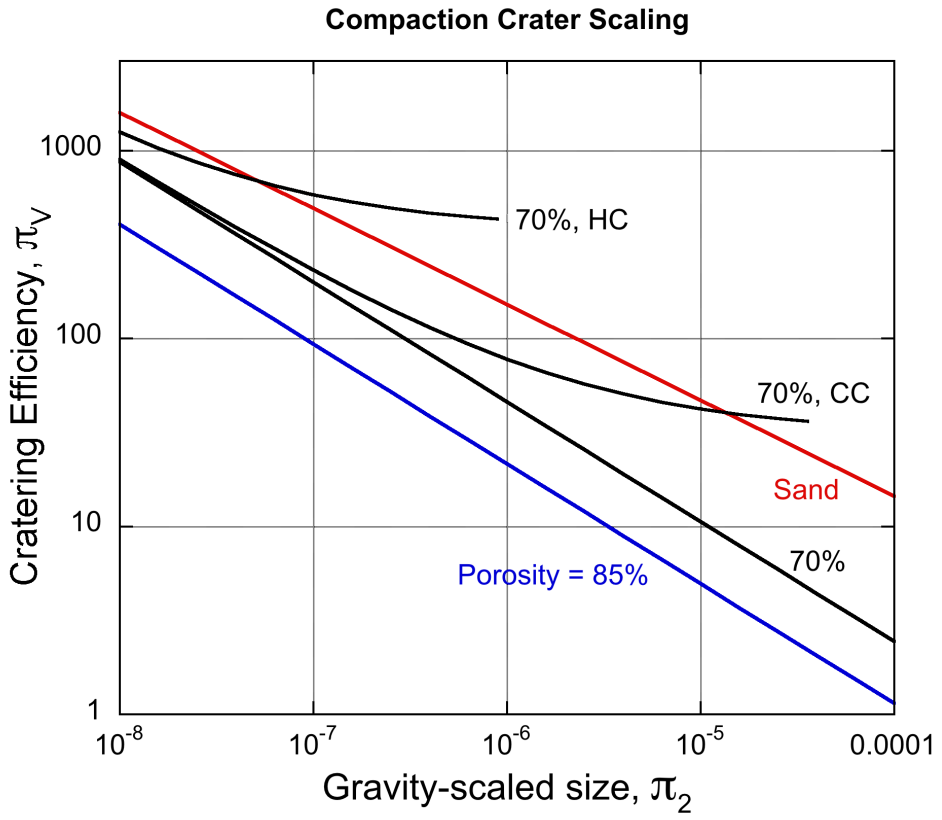

Figure S5. Cratering efficiency comparison between cohesionless regolith (modeled as dry sand) and highly porous granular materials (based on Housen et al., 2018). Porosity generally lowers cratering efficiency (reduces mass excavated and displaced), as illustrated by the gravity-scaled, sloping lines in log-log space. Depending on the value of $Y_c/\rho U^2$, however, crushing and compaction can contribute to crater volume at larger gravity-scaled sizes, counteracting this trend. Such scaling is illustrated for Y_c = 100 kPa, ρ = 500 kg m^{-3}, and the characteristic, or modal, impact speeds for cold classical (CC) and hot classical (HC) Kuiper belt objects onto Arrokoth, 300 and 1400 m s^{-1}, respectively (Greenstreet et al., 2019). The transition to compaction cratering is truncated here at its limit of applicability at right (see Housen et al., 2018); for larger π_2, self-compaction of the target begins to affect the scaling, which was not explicitly developed in Housen et al. (2018).

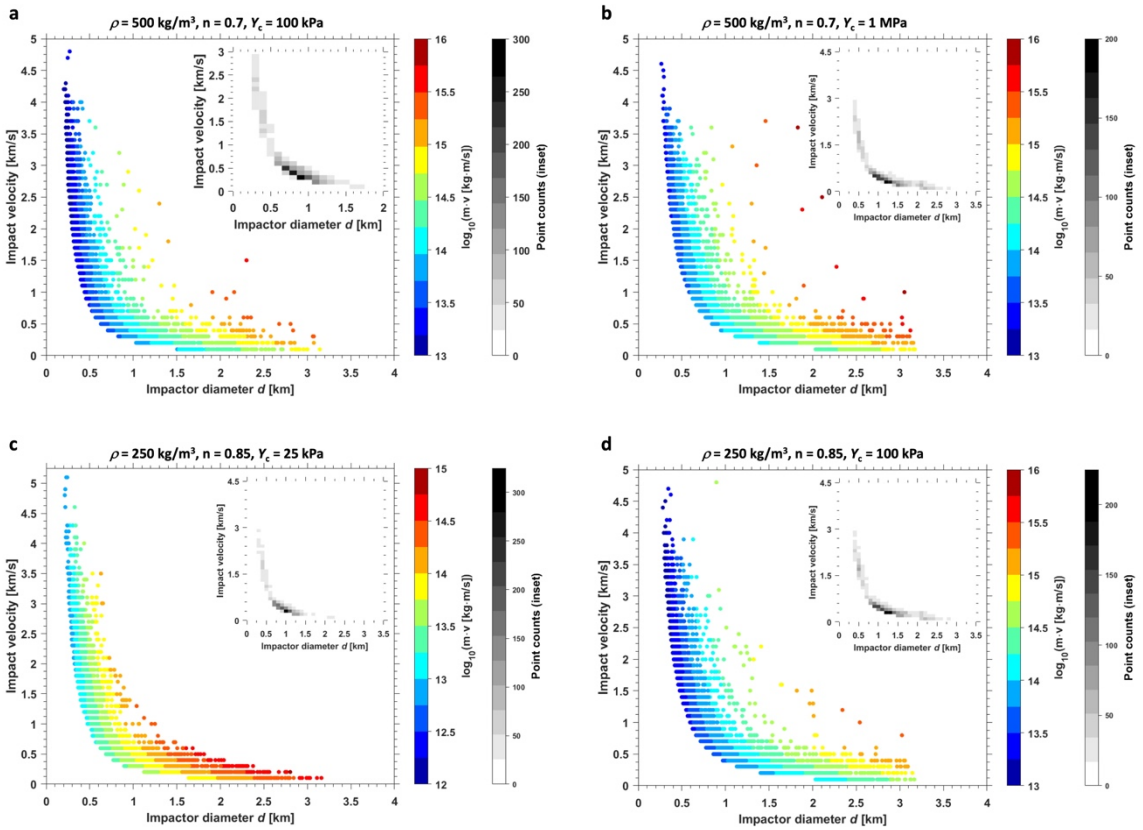

Figure S6. Monte Carlo distribution of impactor sizes and velocities that could have created Sky crater on Arrokoth, for different assumed porosities and crush strengths. a) is identical to Figure 4a of the main text. b) For larger Y_c cratering efficiency goes down (less compaction), necessitating greater impactor momentum and possibility of lobe destabilization. c) and d) Lower impactor and target density naturally imply lower impactor momentum, but similar SL lobe displacements as Arrokoth's mass is reduced in proportion (note different momentum color scales). The most likely impactor momentum input (insets) likely sufficed to break the bond between Arrokoth's two lobes, but as argued in the main text, displacement was limited by dissipation at the crushed and shearing neck between the two. For much larger impactor sizes and momenta (outliers in the Monte Carlo distribution), the two lobes of Arrokoth could have rearranged (cf. Hirabayashi et al., 2020), but this simply did not occur to the actual (IRL) Arrokoth.

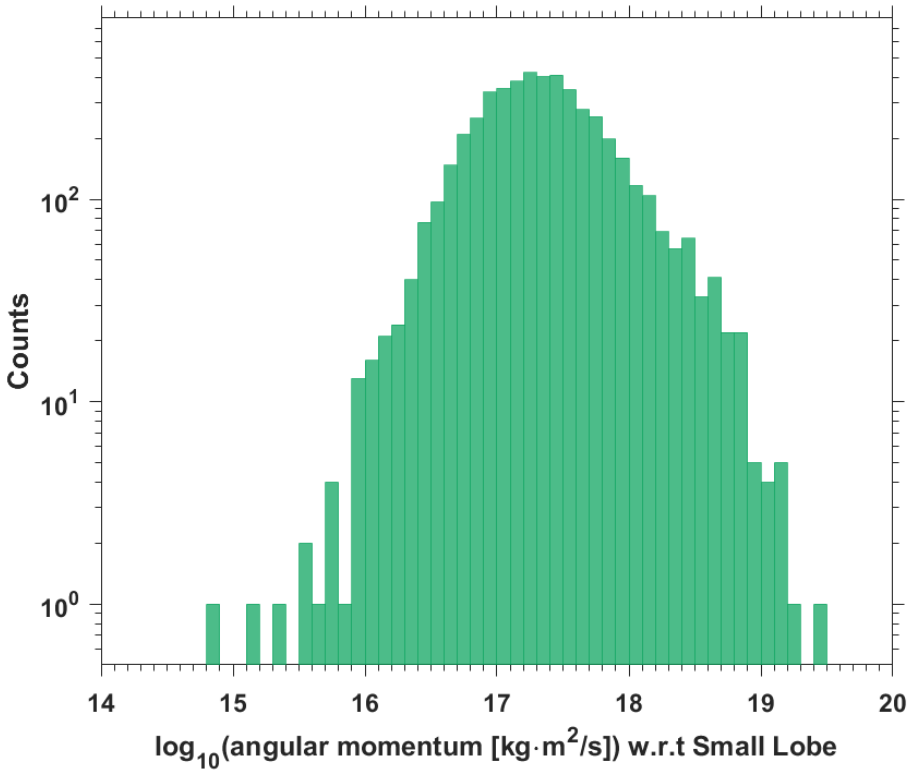

Figure S7. Monte Carlo distribution angular momentum imparted to SL by the Sky-forming impactor, corresponding to the simulation illustrated in Figure 3 of the main text.

References

Bakanova, A. A., Zubarev, V. N., Sutulov, Y.N., & Trunin, R. F. (1976). Thermodynamic properties of water at high pressures and temperatures, *Soviet Physics JETP, English Translation*, 41, 544–548.

Basilevsky, A. T., Krasil'nikov, S. S., Shiryaev, A. A., Mall, U., Keller, H. U., Skorov, Yu. V., et al. (2016). Estimating the strength of the nucleus material of comet 67P Churyumov–Gerasimenko. *Solar System Research*, *50*, 225–234. https://doi.org/10.1134/S0038094616040018

Cooper, M. R., Kovach, R. L., & Watkins, J. S. (1974). Lunar near-surface structure. *Reviews of Geophysics and Space Physics*, *12*, 291–308. https://10.1029/RG012i003p00291

Durham, W. B., McKinnon, W. B., & Stern, L. A. (2005). Cold compaction of water ice. *Geophysical Research Letters*, *32*, L18202. https://doi.org/10.1029/2005GL023484

Greenstreet, S., Gladman, B., McKinnon, W. B., Kavelaars, J. J., & Singer, K. N. (2019). Crater density predictions for New Horizons flyby target 2014 MU69. *Astrophys. J. Lett.*, *872*(1), L5. https://doi.org/doi:10.3847/2041-8213/ab01db

Groussin, O., Jorda, L., Auger, A.-T., Kührt, E., Gaskell, R., Capanna, C., et al. (2015). Gravitational slopes, geomorphology and material strengths of the nucleus of comet 67P/Churyumov-Gerasimenko from OSIRIS observations. *Astronomy & Astrophysics*, *583*, A32. https://doi.org/10.1051/0004-6361/201526379

Hirabayashi, M., Trowbridge, A. J., & Bodewits, D. (2020). The mysterious location of Maryland on 2014 MU69 and the reconfiguration of its bilobate shape. *Astrophysics Journal Letters*, *891*, L12. https://doi.org/10.3847/2041-8213/ab3e74

Housen, K. R., Sweet, W. J., & Holsapple, K. A. (2018). Impacts into porous asteroids. *Icarus*, *300***,** 72-96. https://doi.org/10.1016/j.icarus.2017.08.019

Kieffer, S. W., & Simonds, C. H. (1980). The role of volatiles and lithology in the impact cratering process. *Reviews of Geophysics and Space Physics*, *18*, 143–181. https://10.1029/RG018i001p00143

Mao, X., McKinnon, W. B., Singer, K. N., Keane, J. T., Robbins, S. J., Schenk, P. M., et al. (2021). Merger and spindown of (486958) Arrokoth by collisions. *52nd Lunar and Planetary Science Conference*, abstract #2415. https://www.hou.usra.edu/meetings/lpsc2021/pdf/2415.pdf

McKinnon, W. B., Richardson, D. C., Marohnic, J. C., Keane, J. T., Grundy, W. M., Hamilton, D. P., et al. (2020). The solar nebula origin of (486958) Arrokoth, a primordial contact binary in the Kuiper Belt. *Science*, *367*, eaay6620. https://doi.org/10.1126/science.aay6620

McKinnon, W. B., Glein, C. R., Bertrand, T., & Rhoden, A. R. (2021). Formation, Composition, and History of the Pluto System: A Post-New Horizons Synthesis. In S. A. Stern, J. M. Moore, W. M. Grundy, L. A. Young, & R. P. Binzel (Eds.) *The Pluto System After New Horizons* (pp. 507–543). Tucson: University of Arizona Press. https://doi:10.2458/azu_uapress_9780816540945-ch022

Morbidelli, A., Nesvorný, D., Bottke, W. F., & Marchi, S. (2021). A re-assessment of the Kuiper belt size distribution for sub-kilometer objects, revealing collisional equilibrium at small sizes. *Icarus*, *356*, 114256. https://doi.org/10.1016/j.icarus.2020.114256

O'Rourke, L., Heinisch, P., Blum, J., Fornasier, S., Filacchione, G., Van Hoang, H., et al. (2020). The Philae lander reveals low-strength primitive ice inside cometary boulders. *Nature*, *586*, 697–701. https://doi.org/10.1038/s41586-020-2834-3

Pajola, M., Vincent, J.-B., Güttler, C., Lee, J.-C., Bertini, I., Massironi, M., et al. (2015). Size-frequency distribution of boulders ≥7 m on comet 67P/Churyumov-Gerasimenko. *Astronomy & Astrophysics*, *583*, A37. https://doi.org/10.1051/0004-6361/20152597

Robbins, S. J. & Singer, K. N. (2021) Pluto and Charon impact crater populations: Reconciling different results. *Planetary Science Journal*, *2*, 192. https://doi.org/10.3847/PSJ/ac0e94

Singer, K. N., McKinnon, W. B., Gladman, B., Greenstreet, S., Bierhaus, E. B., Stern, S. A., et al. (2019). Impact craters on Pluto and Charon indicate a deficit of small Kuiper belt objects. *Science*, *363*, 955–959. https://doi.org/10.1126/science.aap8628

Singer, K. N., Greenstreet, S., Schenk, P. M., Robbins, S. J., & Bray, V.J. (2021). Impact craters on Pluto and Charon and terrain age estimates**.** In S. A. Stern, J. M. Moore, W. M. Grundy, L. A. Young, & R. P. Binzel (Eds.) *Pluto System After New Horizons* (pp. 121–145). Tucson: University of Arizona Press. https://doi:10.2458/azu_uapress_9780816540945-ch007

Stesky, R. M. (1978). Experimental compressional wave velocity measurements in compacting powders under high vacuum: applications to lunar crustal sounding. *Proceedings Lunar and Planetary Science Conference 9th*, 3637–3649. New York: Pergamon.